**In your phase! Neural phase synchronization underlies visual imagery of faces**

Andrés Canales-Johnson[1,2,3*§], Renzo C. Lanfranco[4*], Valdas Noreika[1,2], Juan Pablo Morales[5], David Martínez-Pernía[3], Joaquín Valdés[3], Alejandro Ezquerro-Nassar[1], Álvaro Rivera-Rei[3], Tristán A. Bekinschtein[1], Eugenio Rodríguez[5], Srivas Chennu[6,7], Agustín Ibáñez[3,8,9,10,11], and David Huepe[3]

[1]Department of Psychology, University of Cambridge, Cambridge, United Kingdom

[2]Medical Research Council, Cognition and Brain Sciences Unit, Cambridge, United Kingdom

[3]Center for Social and Cognitive Neuroscience, Universidad Adolfo Ibáñez, Santiago, Chile

[4]Department of Psychology, University of Edinburgh, Edinburgh, United Kingdom

[5]School of Psychology, Pontificia Universidad Católica de Chile, Santiago, Chile

[6]School of Computing, University of Kent, Chatham Maritime, United Kingdom

[7]Department of Clinical Neurosciences, University of Cambridge, Cambridge, United Kingdom

[8]Institute of Cognitive and Translational Neuroscience (INCyT), INECO Foundation, Favaloro University, Buenos Aires, Argentina

[9]National Scientific and Technical Research Council (CONICET), Buenos Aires, Argentina

[10]Universidad Autónoma del Caribe, Barranquilla, Colombia

[11]Centre of Excellence in Cognition and its Disorders, Australian Research Council (ACR), Sydney University, NSW, Australia.

*These authors contributed equally to this work

[§]**Correspondence to:** Dr Andrés Canales-Johnson, Department of Psychology, University of Cambridge, Downing Site, CB2 3EB, Cambridge, United Kingdom. Email: afc37@cam.ac.uk

**Funding:** This work was partially supported by grants from CONICET, CONICYT/FONDECYT Regular (1130920 and 1140114), FONCyT-PICT 2012-0412, FONCyT-PICT 2012-1309 and INECO Foundation.

**ABSTRACT**

Mental imagery is the process through which we retrieve and recombine information from our memory to elicit the subjective impression of “seeing with the mind’s eye”. Many studies using imaging and neurophysiological techniques have shown several similarities in brain activity between visual imagery and visual perception. However, currently the dynamics of the brain in response to socially relevant stimuli, like faces, have not been studied. Elucidating brain dynamics during visual imagery of faces may help to understand the role of internal representation of socially relevant stimuli in the brain. Here we used electroencephalography to investigate brain dynamics during visual imagery of faces. We found that internal generation of visually imagined experiences is associated with long-range phase synchronization in gamma frequency band between frontal and parietal electrodes and theta frequency band between frontal electrodes. These results suggest that fronto-parietal gamma phase synchronization may be related to the endogenous binding of facial visual features transiently sustained in memory, whereas the interhemispheric frontal-theta synchrony might be encoding the memory reactivation of face stimuli.

**Keywords:** visual imagery; mental imagery; phase synchrony; brain dynamics; gamma frequency range; theta frequency range

## 1. Introduction

Visual mental imagery—or simply visual imagery—is the process through which we retrieve and recombine information from the long-term memory, resulting in the subjective impression of "seeing with the mind's eye" (Ganis, Thompson, & Kosslyn, 2004). Identification of the neural processes underlying imagery is important both for the understanding of cognition (Ganis, Thompson, Mast, & Kosslyn, 2003; Kosslyn, 2005; Moulton & Kosslyn, 2009) and for the understanding and treatment of certain psychiatric disorders, such as schizophrenia and posttraumatic stress disorder (Holmes & Mathews, 2010; Pearson, Deeprose, Wallace-Hadrill, Heyes, & Holmes, 2013; Pearson, Naselaris, Holmes, & Kosslyn, 2015).

Visual imagery and visual perception have shown to involve the same brain regions (Ishai, Ungerleider, & Haxby, 2000; Kosslyn, Thompson, & Alpert, 1997), exhibiting an spatial overlap that is neither uniform nor complete. Therefore, researchers have suggested that the same sensory networks may be engaged differently by visual imagery and perception (Kosslyn et al., 1999; Mechelli, Price, Friston, & Ishai, 2004). Ganis & Schendan (2008) investigated whether visual perception and visual imagery of faces recruit the same early perceptual processes, as assessed by the event-related potential (ERP) complex N170/vertex positive potential (VPP) using a rapid adaptation paradigm. As expected, face stimuli elicited a robust N170 potential localized to posterior occipito-temporal scalp (as well as a VPP at central sites). However, while perceived adaptors (physical stimuli) diminished ERP amplitude, visualized adaptors (imagined stimuli) enhanced it, suggesting that perceived adaptors modulate high-level sensory regions via bottom-up mechanisms, whereas visualized adaptors affect them via top-down mechanisms. These findings show that visual perception and visual imagery are not identical, even though both engage similar neural processes.

Multiple cognitive processes seem to take part in visual imagery, especially working memory. It has been shown that memory retrieval, working memory, and feature binding are core processes underlying visual imagery (Gyselinckx, Penders, & Vullers, 2007; Hamamé et al., 2012; Jafarpour, Fuentemilla, Horner, Penny, & Duzel, 2014), although precise interactions between these functions and visual imagery remain uncertain. However, while working memory is primarily associated with activation of regions within the frontal cortex (Palva, Monto, Kulashekhar, & Palva, 2010), visuo-spatial working memory involves a broader neural network of occipital and temporal visual areas under executive frontal lobe control (Hamamé et al., 2012).

Working memory of visual mental objects has been associated with increased oscillatory activity in the gamma band in parietal brain regions (Tallon-Baudry & Bertrand, 1999). Visual feature binding is thought to involve the

fusiform gyrus, the dorsal premotor cortex, and several structures within the parietal cortex, as demonstrated by multiple fMRI and TMS studies (Koivisto & Silvanto, 2012; Parra, Della Sala, Logie, & Morcom, 2014; Pollmann, Zinke, Baumgartner, Geringswald, & Hanke, 2014; Shafritz, Gore, & Marois, 2002). Binding of facial features recruits the bilateral middle fusiform gyri and the left precuneus (Boremanse, Norcia, & Rossion, 2013; Kottlow, Jann, Dierks, & Koenig, 2012). Furthermore, Kottlow et al. (2012) reported a link between an increase in gamma synchronization and binding activity during a face integration task. Thus, we can argue that working memory and feature binding literature hypothesize that dynamic network interactions should underlie generation, retrieval, and maintenance of visual mental images, such as faces. However, studies that have addressed the brain network dynamics of visual imagery are still scarce.

A few studies have addressed the neural dynamics of visual imagery. de Borst et al. (2012), for instance, used a combination of EEG and fMRI to investigate large-scale networks involved in visual imagery of complex scenes and found that beta and theta synchronization in frontal regions preceded activation of parietal and occipital regions relative to an auditory control task. This led the authors to propose a model of mental imagery with a "frontal relay station" orchestrating visual imagery of scenes. In a more recent magnetoencephalography (MEG) study, Dijkstra, Mostert, Lange, Bosch, & van Gerven (2018) explored temporal dynamics of category representation (faces and houses) during visual perception and visual imagery. Perception was characterized by high temporal specificity and distinct processing stages, whereas imagery showed wide generalization and low temporal specificity from the onset of stimulus/image, with an overlap between perception and imagery starting around 130 ms, then decreasing around 210 ms, and increasing again from 300 ms after stimulus/image onset – it takes longer time to generate visual representations of mental imagery based on purely top-down processes that either do not rely on early perceptual representations, or such representations are transient and variable over time.

Here, we characterize the brain dynamics of visual imagery of faces by using EEG phase-synchrony and spectral power analysis in the delta to gamma frequency range (1-60 Hz). Based on studies reporting theta coherence in the frontal lobes as a key EEG signature of working memory (Hamamé et al., 2012; Kopp, Schröger, & Lipka, 2004; Schack, Vath, Petsche, Geissler, & Möller, 2002), we predict that visual imagery of faces will be associated with frontal interhemispheric synchronization in the theta frequency range. Furthermore, given that visual imagery is driven by top-down modulation of sensory regions (Dijkstra, Zeidman, Ondobaka, Gerven, & Friston, 2017; Ganis & Schendan, 2008), whereas central maintenance of visual representations involves gamma synchronization (Palva et al., 2010), we also predict that visual imagery of faces will be associated with gamma

phase synchronization within fronto-parietal network. Therefore, altogether, we predict that the temporal dynamics of visual imagery of faces will involve two distinguishable processes: (i) memory retrieval of faces associated with frontal theta synchronization, and (ii) binding of facial features associated with fronto-parietal gamma synchronization.

## 2. Methods

### 2.1. Participants

Twenty-one right-handed participants (12 male; mean age = 21.20 years) with normal or corrected-to-normal vision, no history of psychiatric or neurological disorders, and no current use of any psychoactive medications, took part in the experiment. All signed an informed consent accepting their participation in the study in accordance with the Declaration of Helsinki and approved by the institutional ethics committee of the Faculty of Psychology of Universidad Diego Portales (Chile).

### 2.2. Stimuli

Stimuli were 10 grayscale images of faces, 1 grayscale image of an oval, and 10 words, each presented on a black background. All face images were full-front views of celebrities with clothing, backgrounds, and hair removed (see Fig. 1 for an example and Supplementary Figure 1). The word stimuli were the 10 names of the corresponding celebrities, presented in a black background in Helvetica font. Participants sat 100 cm from the monitor. Face images (7.32 × 8.87 cm) were presented inside an oval that subtended ~4.19 × 5.08° of visual angle. For a description of stimuli validation, see Supplementary material. Stimuli were presented on a 17-inch LCD monitor using Python and Pygame software.

### 2.3. Procedure

We used a modified version of the paradigm developed by Ganis & Schendan (2008) with three experimental blocks (240 trials per condition): control condition, visual imagery practice, and visual imagery condition. In the control condition (Fig. 1, left), after seeing a name of a celebrity for 300 ms, participants were asked to press a key after seeing a grey oval on the center of the screen. Then, 200 ms after the key press, a test face appeared (300 ms) which was congruent with the name of the celebrity presented before. The imagery practice started

with memorization of pictures of 10 faces of celebrities with 12 exposures for each. Next, participants practiced mentally visualizing each memorized picture three times. During the imagery practice block, the name appeared followed by a black screen with a gray oval centered in the middle of the screen where participants visualized the picture of the named face. Having done so, they pressed a key to see the actual picture in order to adjust their mental image. In the imagery condition (Fig. 1, right), the name of a celebrity appeared for 300 ms followed by a black screen with a middle-centered gray oval where subjects mentally visualized the associated memorized picture. Participants were instructed to generate a mental image of the face cued by the celebrity's name shown and project said mental image onto the grey oval on the screen. As soon as their mental image was very clear, they had to press a key, for which task they could not exceed 10 seconds, or the trial would be interrupted, and the experiment would move to the next trial. Then, 200 milliseconds after the key press the test picture appeared for 300 ms. For all trials, the test picture was the picture of the face that was visualized mentally. There were 240 trials per condition. After each imagery trial, participants were asked to rate the vividness, contour definition, emotional expression, and contrast on a 1-5 Likert scale.

**2.4. Electrophysiological recordings and analysis**

EEG signals were recorded with 129-channels HydroCel Sensors using a GES300 Electrical Geodesic amplifier at a rate of 500 Hz, and NetStation software. The physical filters were set at 0.01–100 Hz for the recording acquisitio, during which Cz electrode was used as reference. For the analyses, the electrodes' average was used as the reference electrode. Two bipolar derivations were designed to monitor vertical and horizontal ocular movements. Eye movement contamination and other artifacts were removed from data before further processing using independent component analysis (Delorme & Makeig, 2004). Continuous data was epoched from -1500 to 0 ms around the button press (0 ms).

Trials that contained voltage fluctuations exceeding ± 200 µV, transients exceeding ± 100 µV, or electro-oculogram activity exceeding ± 70 µV were rejected. After screening, no significant differences in the number of trials were observed between conditions: each of them yielded at least 91% of artifact-free trials which represented a minimum of 210 trials per condition. In order to address the sample size biased imposed by our phase locking measure (see below), we used the same number of trials for all conditions and participants by randomly selecting 210 artifact-free trials in those conditions that exceeded this minimum. The EEGLAB MATLAB toolbox was used for data pre-processing and pruning (Delorme & Makeig, 2004).

**2.5. Analysis of endogenous EEG activity related to visual imagery.**

There is growing evidence that endogenous or ''ongoing'' neural activity, i.e. activity that is not time-locked to stimuli, is neither meaningless nor random but that it carries functional significance (Freeman, 2000). A classical experimental approach for studying endogenous changes in the EEG related to internal fluctuations during cognitive tasks is to analyze the EEG window *before* the onset of motor responses when participants report internal changes. For instance, this approach has been used for studying neural signatures of bistable awareness (Britz, Landis, & Michel, 2009; Canales-Johnson et al., 2019; Parkkonen, Andersson, Hämäläinen, & Hari, 2008), binocular rivalry (Doesburg, Kitajo, & Ward, 2005) and intrusions of consciousness (Noreika et al., 2015). Following the same rationale, but this time for the analysis of visually *imagined* faces, we computed ongoing EEG activity preceding the onset of each response (button press), i.e. response-locked activity. We performed two separate analyses: one that captures local synchrony (spectral power) and a second analysis that captures long-range synchrony (phase synchrony) between signals in relation to visual imagery (described below in full).

In order to determine the length of the EEG window of analysis, we identified the trial with the shortest reaction time relative to the onset of the grey oval for both the control (1760 ms) and the visual imagery conditions (2870 ms). Our criteria for making conditions comparable was that the grey oval should be present during the entire window of analysis. Thus, we decided to use a window of 1500 ms for all trials and conditions (from -1500 to 0 ms locked to the response time). Time-frequency charts of spectral power and phase-synchrony are expressed in z-scores relative to a baseline period (-1500 to -1250 ms).

### 2.6. Between-electrodes measure: long-range phase synchronization

We quantified phase locking between pairs of electrodes to measure dynamical interactions among electrodes oscillating in the same frequency band. Phase synchronization analysis proceeds in two steps: (i) estimation of the instantaneous phases and (ii) quantification of the phase locking.

#### 2.6.1. Estimation of the instantaneous phases

To obtain the instantaneous phases, $\varphi$, of the neural signals, we used the Hilbert transform approach (David, Cosmelli, & Friston, 2004). The analytic signal $\xi(t)$ of the univariate measure $x(t)$ is a complex function of continuous time $t$ defined as

(1) $\xi(t) = x(t) + ix_h(t) = a_\xi(t)e^{i\varphi\xi(t)}$

where the function $x_h(t)$ is the Hilbert transform of $x(t)$

(2) $x_h(t) = \frac{1}{\pi} P.V. \int_{-\infty}^{+\infty} \frac{x(t)}{t-\tau} d\tau$

P.V. indicates that the integral is taken in the sense of Cauchy principal value. Sequences of digitized values give a trajectory of the tip of a vector rotating counterclockwise in the complex plane with elapsed time.

The vector norm at each digitizing step $t$ is the state variable for instantaneous amplitude $a_\xi(t)$. This amplitude corresponds to the length of the vector specified by the real and imaginary part of the complex vector computed by Pythagoras' law and is equivalent to the magnitude of the observed oscillation at a given time and frequency point.

(3) $a_\xi(t) = \sqrt{x(t)^2 + ix_h(t)^2}$

is the arctangent of the angle of the vector with respect to the real axis and is the state variable for instantaneous phase $\varphi_x(t)$.

(4) $\varphi_x(t) = arctg \frac{ix_h(t)}{x(t)}$

The instantaneous phase $\varphi_x(t)$ of $x(t)$ is taken to be equal to $\varphi_\xi(t)$. Identically, the phase $\varphi_y(t)$ is estimated from $y(t)$. This phase is thus the angle of the vector specified by the real and imaginary components. For a given time and frequency point, it corresponds to a position inside the oscillation cycle (peak, valley, rising, or falling slope).

The instantaneous phase, although defined uniquely for any kind of signal to which the Hilbert transform can be applied, is difficult to interpret physiologically for broadband signals. For this reason, a standard procedure is to consider only narrow-band phase synchronization by estimating an instantaneous phase for successive frequency bands, which are defined by band-pass filtering the time series (Le Van Quyen et al., 2001). Thus, we

bandpass filtered EEG signals in multiple successive 1 Hz-wide frequency bins from 1 to 60 Hz using a zero-phase shift non-causal finite impulse filter.

### 2.6.2. Phase locking quantification: weighted phase lag index (wPLI)

Phase synchronization can be considered as an EEG measure of information exchange between neuronal populations (Chennu et al., 2014). Generally speaking, phase synchronization is calculated from the phase or the imaginary component of the complex cross-spectrum between signals measured at a pair of channels. For example, the well-known Phase Locking Value (PLV; see Lachaux, Rodriguez, Martinerie, & Varela, (1999)) is obtained by averaging the exponential magnitude of the imaginary component of the cross-spectrum. However, many of such phase coherence indices derived from EEG data are affected by the volume conduction (Nunez & Srinivasan, 2006). As a result, a single dipolar source can produce spurious coherence between spatially disparate EEG channels, rather than the values being related to a pair of distinct interacting sources per se. The Phase Lag Index (PLI), first proposed by Stam, Nolte, & Daffertshofer (2007), attempts to minimize the impact of volume conduction and common sources inherent in EEG data by averaging the signs of phase differences, thereby ignoring average phase differences of 0 or 180 degrees. This is based on the rationale that such phase differences are likely to be generated by volume conduction of single dipolar sources. Despite being insensitive to volume conduction, PLI has two important limitations: first, there is a strong discontinuity in the measure, which causes it to be maximally sensitive to noise; second, when calculated on small samples, PLI is biased toward strong coherences (i.e., it has a positive sample-size bias). The Weighted PLI measure (wPLI; see (Vinck, Oostenveld, van Wingerden, Battaglia, & Pennartz, 2011)) addresses the former problem by weighting the signs of the imaginary components by their absolute magnitudes. The PLI sample size problem can be addressed by considering the same amount of trials per condition in the phase coherence analysis (see Electrophysiological recordings and analysis section in Methods). Further, as the calculation of wPLI also normalizes the weighted sum of signs of the imaginary components by the average of their absolute magnitudes, it represents a dimensionless measure of connectivity that is not directly influenced by differences in spectral or cross-spectral power. For these reasons, we employed wPLI to estimate connectivity in our data. The wPLI index ranges from 0 to 1, with a value of 1 indicating perfect synchronization (phase difference is perfectly constant throughout the trials) and value 0 representing total absence of synchrony (phase differences are random).

### 2.7. Within-electrodes measure: spectral power

The spectral power was estimated by calculating the square of the envelope obtained from the absolute value of the Hilbert transform per frequency bin (i.e. from 1 to 60 Hz). This procedure provides the instantaneous power emission which reflects the strength of local synchronization.

### 2.8. Selection of electrodes of interest

Groups of electrodes were selected for spectral power analysis (within-electrodes measure) and phase synchrony analysis (between-electrodes measure) by selecting canonical frontal and parietal electrodes. In the case of the spectral gamma power analysis, power values within frontal and parietal electrodes were averaged per condition and participant. Similarly, for spectral theta power, values within frontal electrodes were averaged per condition and participant. In the case of fronto-parietal wPLI analysis, we calculated the mean connectivity that every electrode of the frontal cluster shared with every electrode of the parietal cluster. Connectivity values between frontal pairs of electrodes and between parietal pairs of electrodes were discarded from the analysis. Similarly, in the case of interhemispheric fronto-frontal wPLI analysis, we calculated the mean connectivity that every electrode of the right-frontal hemisphere shared with every electrode of the left-frontal hemisphere discarding connectivity values between right-frontal electrodes and between left-frontal electrodes. This procedure allows to test specifically the role of long-distance interactions (fronto-parietal and interhemispheric fronto-frontal pairs of electrodes) during visual imagery. Finally, wPLI values of the corresponding regions of interest were averaged per condition.

### 2.9. Statistical analysis

For EEG results, a cluster-based nonparametric statistical framework implemented in FieldTrip (Oostenveld, Fries, Maris, & Schoffelen, 2011) was used throughout the analysis of the power and wPLI time-frequency charts. In brief, time-frequency windows of interest were compared in pairs of experimental conditions (control vs. imagery). For each such pairwise comparison, epochs in each condition were averaged subject-wise. These averages were passed to the analysis procedure of FieldTrip, the details of which are described elsewhere (Maris & Oostenveld, 2007). In short, this procedure compared corresponding time-frequency points in the subject-wise averages using one-tailed dependent (for within-subject comparisons) or independent (for between-subject comparisons) samples *t*-tests. Although this step was parametric, FieldTrip uses a nonparametric clustering method (Bullmore et al., 1999) to address the multiple comparisons problem. *t* values of adjacent time-frequency points whose *P* values were lower than 0.05 were clustered together by summating their *t*

values, and the largest such cluster was retained. This whole procedure, i.e., calculation of *t* values at each time-frequency point followed by clustering of adjacent *t* values, was then repeated 1000 times, with recombination and randomized resampling of the subject-wise averages before each repetition. This Monte Carlo method generated a nonparametric estimate of the *p*-value representing the statistical significance of the originally identified cluster. The cluster-level *t* value was calculated as the sum of the individual *t* values at the points within the cluster.

## 3. Results

### 3.1. Behavioral analysis

Pairwise comparisons revealed a significant difference in reaction times between visual imagery (M = 4603, SD = 1043 ms) and control (M = 2550 ms, SD = 614 ms) conditions (t(1,20) = 8.83). We did not find any significant relationship between subjective ratings with phase synchronization or with spectral power in the theta or gamma ranges.

### 3.2. Long-distance phase synchrony patterns related to imagery.

Between fronto-parietal electrodes (Fig. 2D), phase synchronization in the gamma band (30-60 Hz) was significantly different between imagery and control conditions during mental imagery (Fig. 2). Cluster-based nonparametric analysis showed a significant cluster from -346 to -194 ms in the gamma range (34-60 Hz; cluster $t$ = 2269; $p$ = 0.018; Fig. 2C). Interestingly, no significant clusters were found between conditions in the spectral power of gamma frequency range in this time-frequency window (Supplementary Figure 2).

Furthermore, phase synchronization in theta band (5-7 Hz) also increased during the mental imagery period in the imagery condition from -998 to -330 ms between interhemispheric fronto-frontal pairs of electrodes (cluster $t$ = 1236, $p$ = 0.019; Fig. 3). As for gamma band activity, no significant cluster of activation was found in the spectral power of theta frequency range between conditions in the same time- frequency window (Supplementary Figure 3).

These findings indicate that visual imagery is associated with an increase in gamma and theta phase-synchronization, but the conditions do not differ in the spectral power of gamma and theta frequency bands.

## 4. Discussion

When we imagine a known face, we first need to recall it to visualize it. Here we show that visual imagery of faces involves EEG phase synchronization when contrasted with a control condition of seeing an oval figure. Our mental imagery task ignited theta phase synchronization among anterior electrodes within a time window from -998 to -330 ms and gamma phase synchronization among frontal and parietal electrodes within a time window from -346 to -194 ms before participants reported their mental image was subjectively clear. We interpret these findings as neural signatures of (1) maintenance of visual representation of known faces in working memory and (2) binding of facial features, correspondingly. We base this interpretation on previous studies about visual representation in the working memory (Palva et al., 2010; Tallon-Baudry & Bertrand, 1999) and binding of facial features (Kottlow et al., 2012; Rodriguez et al., 1999).

The increase in the synchronization of theta frequency range among anterior electrodes during imagery may be related to reactivation of face memories and identification of imagined faces (Kim et al., 2012; Sauseng, Griesmayr, Freunberger, & Klimesch, 2010) as recognition of previously viewed objects has been associated with an increase of theta synchronization (Kim et al., 2012) given that fronto-parietal gamma synchronization onset (Fig. 2C) temporally followed the offset of the frontal theta cluster (Fig. 3C). The temporal order of these results can suggest that fronto-parietal gamma phase synchronization may be related to the endogenous binding of facial visual features transiently sustained in memory, whereas interhemispheric frontal-theta synchrony might be related to memory reactivation of a known face.

It is worth noting that spectral power of theta and gamma bands did not differ between conditions. Few studies have reported on changes in gamma or theta power and its temporal dynamics associated with visual binding or episodic memory tasks. (Nyhus & Curran, 2010; Tallon-Baudry & Bertrand, 1999; Tallon-Baudry, Bertrand, Delpuech, & Pernier, 1996). However, there have been reports of increased local synchronization in the beta and gamma frequencies during visual binding. Melloni et al. (2007), for example, found that this increase occurs specifically during preconscious processing stages of visual input in a bottom-up manner and therefore does not necessarily result in conscious detection. We hypothesize that because mental imagery is a top-down, consciously driven process (Dijkstra et al., 2017; Mechelli et al., 2004), it is not accompanied by the changes in local power that characterize other visual tasks. A complementary hypothesis is that the apparent discrepancy in gamma power findings between perceptual tasks and imagery tasks may reflect the neural distinction between

exogenously driven and endogenously driven binding processes. Such a hypothesis would predict that the signature of endogenous binding is not gamma range intensity (i.e. power), but cross-channel synchronization.

Notably, it has also been shown that induced gamma activity in scalp EEG can reflect micro-saccadic eye movements (Yuval-Greenberg, Tomer, Keren, Nelken, & Deouell, 2008), while visual imagery tasks typically facilitate involuntary saccades (Mast & Kosslyn, 2002). To control for the possibility that increased gamma phase synchronization in the imagery condition might have been due to eye movements, spectral power analysis was carried out for gamma frequencies in the same time window. However, absence of gamma power differences between conditions suggests that coherence results cannot be attributed to eye movements.

This study was concerned with the neural mechanisms underlying visual imagery of faces, including those that overlap with normal face perception. Thus, our control condition was devised so that it did not include a face as the test stimulus but rather featured a grey oval, identical to the one employed in the imagery condition. This meant that both conditions consisted of the exact same stimuli with the manipulation being only in the instructions given to subjects in each condition. Although it is likely that attentional resources were deployed while waiting for the grey oval to appear in the control condition, those same resources were presumably deployed during the imagery condition, and therefore we have no reason to believe that the differences reported in this study can be attributed to attentional processes.

It could be argued that the results can be explained by a repetition effect and/or a memory effect rather than by imagery, as imagery condition is always preceded by the imagery practice session. However, it is a well-established fact that when stimuli are repeated, neural activity is usually reduced (Grill-Spector, Henson, & Martin, 2006). For instance, some studies report decreased gamma band frequency power (> 30 Hz) around 220–350 ms for repetition of familiar objects across lags of one or two intervening objects (Gruber & Müller, 2005). On the contrary, active retention and encoding of one or more items in working memory have generally been associated with increase in theta and gamma power (Jacobs & Kahana, 2009; Jokisch & Jensen, 2007; Meltzer et al., 2008). Thus, a repetition effect would imply a decrease in theta and gamma amplitudes whereas a memory effect, an increase in amplitude in these frequency bands in the imagery condition relative to control. However, both possibilities were excluded because theta and gamma amplitudes did not change during the time windows where phase-synchrony increased. Even thus, future studies on neural dynamics of visual imagery should address this matter directly. Interestingly, the dynamical process underlying visual imagery can be

inferred due to the excellent temporal resolution provided by the Hilbert transform (see Materials and Methods).

Our findings complement and expand what has been reported about the brain dynamics of visual imagery in the study by Dijkstra et al. (2018). While they employed raw voltage values to describe the temporal dynamics of visual imagery using category representations as predictors, we employed a connectivity measure. More specifically, they measured the multivariate relationship between electrodes using voltage values while we tested a specific hypothesis about the communication between channels, measured as EEG phase synchronization (wPLI). Thus, we distinguished between a mechanism associated to visual imagery binding and a different mechanism associated to working memory, a distinction that to our knowledge had not been made empirically in the brain dynamics of visual imagery until now.

However, our study presents a few limitations that could be addressed in the future. First, our results reflect dynamic changes with clear topographic distributions. However, future studies could source-reconstruct the EEG signals to link neural dynamic findings to brain sources. Second, our conclusions require reverse inference based on past studies and temporal occurrence given the straightforward approach of our visual imagery task. Future studies could include additional behavioral tasks that can allow distinguishing between memory retrieval, memory maintenance, and binding of facial features.

Overall, the present study indicates that the imagery of faces is associated with spatially broad phase synchronization in the gamma and theta frequency ranges, arguably involving face memory-retrieval, feature binding, visual recognition, and working memory maintenance functions. These findings suggest that some electrophysiological correlates of mental imagery coincide with EEG phase synchrony earlier reported to be associated with visual perception and memory, while others seem to be unique to mental imagery.

**Figure Legends**

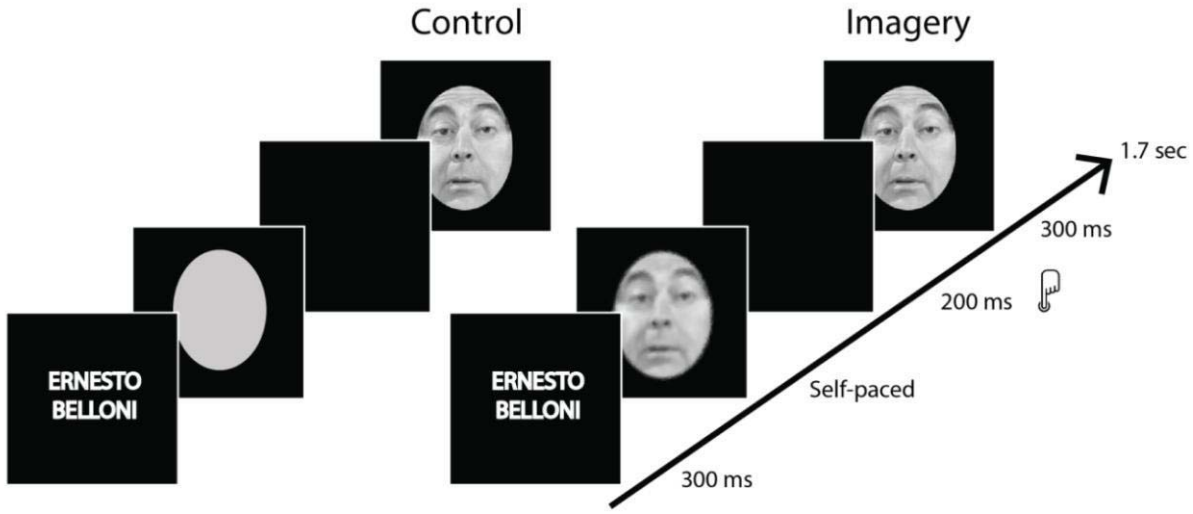


**Fig. 1.** Diagram of an experimental trial for the visual imagery and control conditions**.** Visual imagery and control conditions had a parallel structure. In the visual imagery condition (the right side of the figure), a celebrity face was visualized mentally after seeing the corresponding name which was presented for 300 ms. Participants pressed a key as soon as they had generated a vivid mental image, and 200 ms after this key press, a test face appeared for 300 ms which was of the same person whose face has been mentally visualized before. In the control condition (the left side of the figure), after seeing a name of a celebrity, participants were asked to press a key after seeing a grey oval on the screen. Then, 200 ms after the key press, a test face appeared (300 ms) which was congruent with the name of the celebrity presented before as a feedback to the participant.

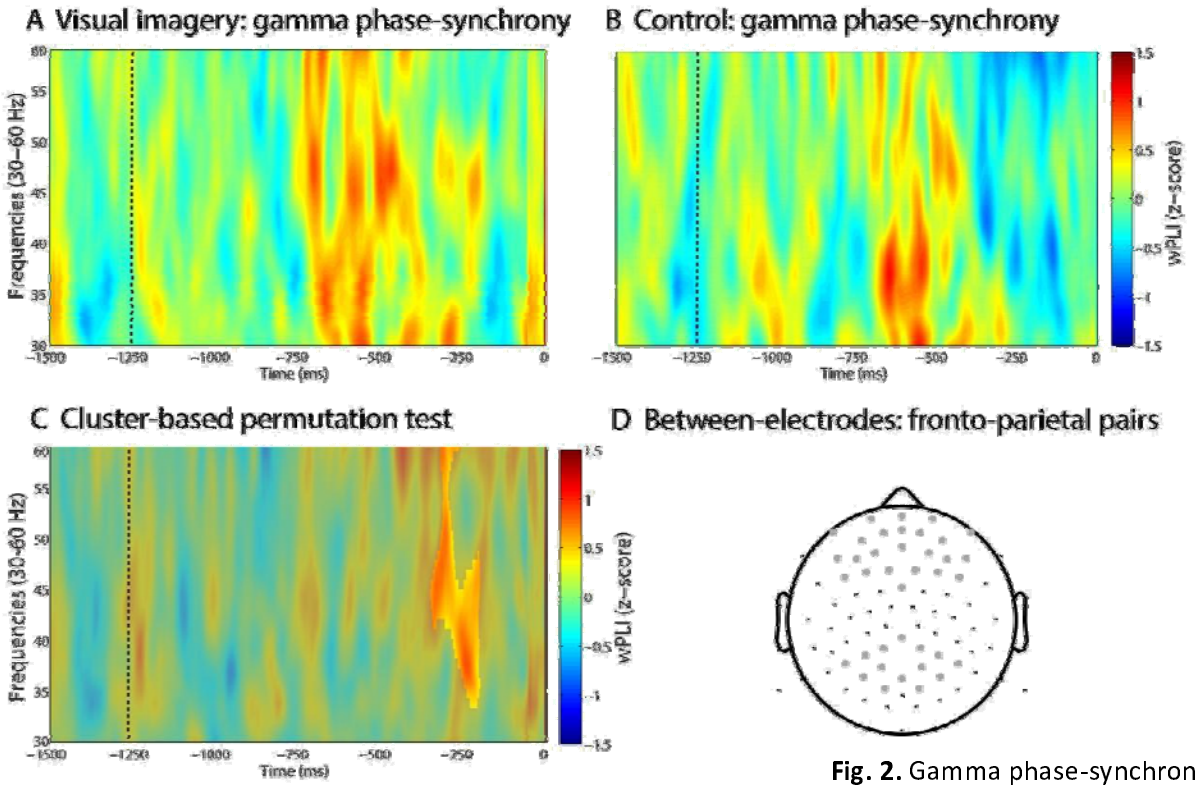


**Fig. 2.** Gamma phase-synchrony between frontal and parietal electrodes. Gamma wPLI (30-60 Hz) for visual imagery **(A)** and control **(B)** conditions. **(C)** Cluster-based permutation test comparing visual imagery and control conditions. The area highlighted in the time-frequency chart depicts a significant wPLI cluster between conditions (p = 0.019, visual imagery minus control). **(D)** Fronto-parietal pairs of electrodes used for calculating wPLI are shown in grey (see Materials and Methods for details). All values are expressed in standard deviations (SD) in reference to the baseline (-1500 to -1250 ms). Trial length (-1500 ms) is relative to response time (0 ms).

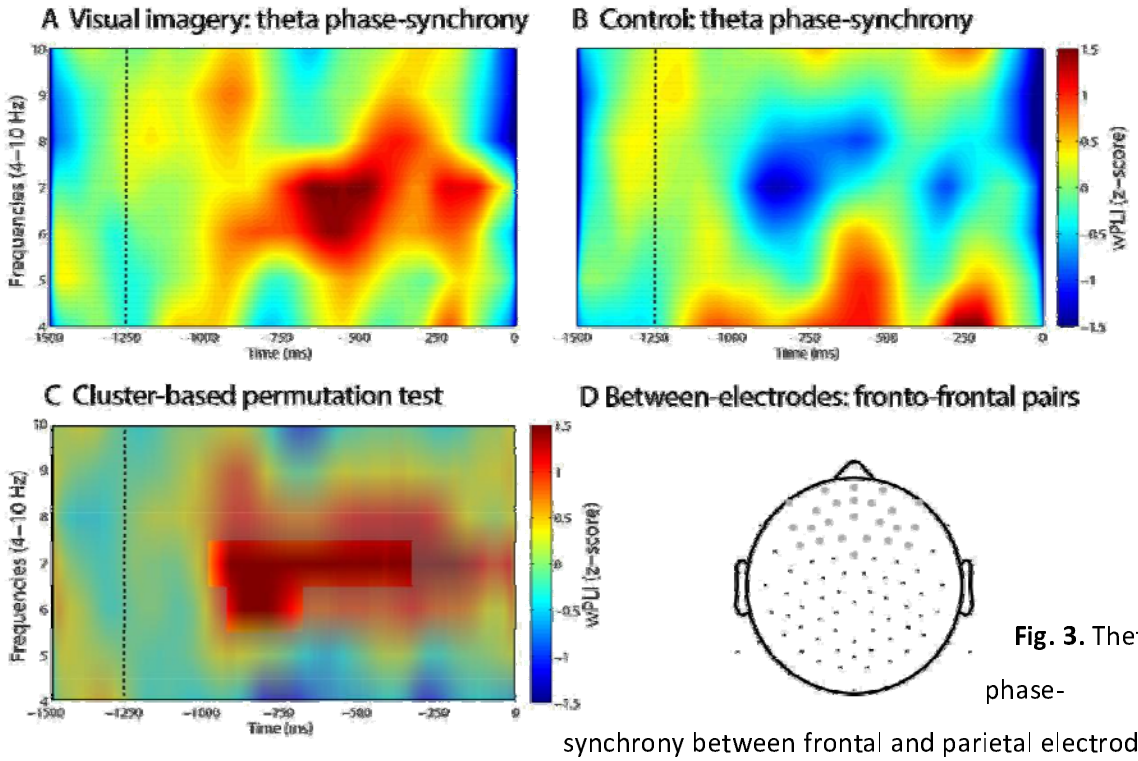


**Fig. 3.** Theta phase-synchrony between frontal and parietal electrodes. wPLI (4-10 Hz) for visual imagery **(A)** and control **(B)** conditions. **(C)** Cluster-based permutation test comparing visual imagery and control. The area highlighted in the time-frequency chart depicts a significant wPLI cluster between conditions (p = 0.019, visual imagery minus control) in the theta band (4-7 Hz). **(D)** Region of interest (ROI) for phase-synchrony analysis. Only interhemispheric fronto-frontal pairs of channels were considered for the analysis (see Materials and Methods for details). All values are expressed in standard deviations (SD) in reference to the baseline (-1500 to -1250 ms). Trial length (-1500 ms) is relative to response time (0 ms).

**REFERENCES**


Boremanse, A., Norcia, A. M., & Rossion, B. (2013). An objective signature for visual binding of face parts in the human brain. *Journal of Vision*, *13*(11), 6–6. https://doi.org/10.1167/13.11.6

Britz, J., Landis, T., & Michel, C. M. (2009). Right Parietal Brain Activity Precedes Perceptual Alternation of Bistable Stimuli. *Cerebral Cortex*, *19*(1), 55–65. https://doi.org/10.1093/cercor/bhn056

Bullmore, E. T., Suckling, J., Overmeyer, S., Rabe-Hesketh, S., Taylor, E., & Brammer, M. J. (1999). Global, voxel, and cluster tests, by theory and permutation, for a difference between two groups of structural MR images of the brain. *IEEE Transactions on Medical Imaging*, *18*(1), 32–42.

Canales-Johnson, A., Billig, A., Olivares, F., González, A., García, M. del C., Silva, W., … Bekinschtein, T. (n.d.). Dissociable neural information dynamics of perceptual integration and differentiation during bistable perception. *BioRxiv*. https://doi.org/10.1101/133801v2

Chennu, S., Finoia, P., Kamau, E., Allanson, J., Williams, G. B., Monti, M. M., … Bekinschtein, T. A. (2014). Spectral Signatures of Reorganised Brain Networks in Disorders of Consciousness. *PLOS Computational Biology*, *10*(10), e1003887. https://doi.org/10.1371/journal.pcbi.1003887

David, O., Cosmelli, D., & Friston, K. J. (2004). Evaluation of different measures of functional connectivity using a neural mass model. *NeuroImage*, *21*(2), 659–673. https://doi.org/10.1016/j.neuroimage.2003.10.006

de Borst, A. W., Sack, A. T., Jansma, B. M., Esposito, F., de Martino, F., Valente, G., … Formisano, E. (2012). Integration of “what” and “where” in frontal cortex during visual imagery of scenes. *NeuroImage*, *60*(1), 47–58. https://doi.org/10.1016/j.neuroimage.2011.12.005

Delorme, A., & Makeig, S. (2004). EEGLAB: an open source toolbox for analysis of single-trial EEG dynamics including independent component analysis. *Journal of Neuroscience Methods*, *134*(1), 9–21. https://doi.org/10.1016/j.jneumeth.2003.10.009

Dijkstra, N., Zeidman, P., Ondobaka, S., Gerven, M. A. J. van, & Friston, K. (2017). Distinct Top-down and Bottom-up Brain Connectivity During Visual Perception and Imagery. *Scientific Reports*, *7*(1), 5677. https://doi.org/10.1038/s41598-017-05888-8

Dijkstra, Nadine, Bosch, S. E., & Gerven, M. A. J. van. (2017). Vividness of Visual Imagery Depends on the Neural Overlap with Perception in Visual Areas. *Journal of Neuroscience*, *37*(5), 1367–1373. https://doi.org/10.1523/JNEUROSCI.3022-16.2016

Dijkstra, Nadine, Mostert, P., Lange, F. P. de, Bosch, S., & van Gerven, M. A. (2018). Differential temporal dynamics during visual imagery and perception. *ELife*, *7*. https://doi.org/10.7554/eLife.33904

Doesburg, S. M., Kitajo, K., & Ward, L. M. (2005). Increased gamma-band synchrony precedes switching of conscious perceptual objects in binocular rivalry. *Neuroreport*, *16*(11), 1139–1142.

Freeman, W. (2000). *Neurodynamics: An Exploration in Mesoscopic Brain Dynamics*. Retrieved from //www.springer.com/gb/book/9781852336165

Ganis, G., & Schendan, H. E. (2008). Visual mental imagery and perception produce opposite adaptation effects on early brain potentials. *NeuroImage*, *42*(4), 1714–1727. https://doi.org/10.1016/j.neuroimage.2008.07.004

Ganis, G., Thompson, W. L., & Kosslyn, S. M. (2004). Brain areas underlying visual mental imagery and visual perception: an fMRI study. *Cognitive Brain Research*, *20*(2), 226–241. https://doi.org/10.1016/j.cogbrainres.2004.02.012

Ganis, G., Thompson, W. L., Mast, F. W., & Kosslyn, S. M. (2003). Visual imagery in cerebral visual dysfunction. *Neurologic Clinics*, *21*(3), 631–646. https://doi.org/10.1016/S0733-8619(02)00097-X

Grill-Spector, K., Henson, R., & Martin, A. (2006). Repetition and the brain: neural models of stimulus-specific effects. *Trends in Cognitive Sciences*, *10*(1), 14–23. https://doi.org/10.1016/j.tics.2005.11.006

Gruber, T., & Müller, M. M. (2005). Oscillatory Brain Activity Dissociates between Associative Stimulus Content in a Repetition Priming Task in the Human EEG. *Cerebral Cortex*, *15*(1), 109–116. https://doi.org/10.1093/cercor/bhh113

Gyselinckx, B., Penders, J., & Vullers, R. (2007). Potential and challenges of body area networks for cardiac monitoring. *Journal of Electrocardiology*, *40*(6), S165–S168. https://doi.org/10.1016/j.jelectrocard.2007.06.016

Hamamé, C. M., Vidal, J. R., Ossandón, T., Jerbi, K., Dalal, S. S., Minotti, L., … Lachaux, J.-P. (2012). Reading the mind's eye: Online detection of visuo-spatial working memory and visual imagery in the inferior temporal lobe. *NeuroImage*, *59*(1), 872–879. https://doi.org/10.1016/j.neuroimage.2011.07.087

Holmes, E. A., & Mathews, A. (2010). Mental imagery in emotion and emotional disorders. *Clinical Psychology Review*, *30*(3), 349–362. https://doi.org/10.1016/j.cpr.2010.01.001

Ishai, A., Ungerleider, L. G., & Haxby, J. V. (2000). Distributed Neural Systems for the Generation of Visual Images. *Neuron*, *28*(3), 979–990. https://doi.org/10.1016/S0896-6273(00)00168-9

Jacobs, J., & Kahana, M. J. (2009). Neural Representations of Individual Stimuli in Humans Revealed by Gamma-Band Electrocorticographic Activity. *Journal of Neuroscience*, *29*(33), 10203–10214. https://doi.org/10.1523/JNEUROSCI.2187-09.2009

Jafarpour, A., Fuentemilla, L., Horner, A. J., Penny, W., & Duzel, E. (2014). Replay of Very Early Encoding Representations during Recollection. *Journal of Neuroscience*, *34*(1), 242–248. https://doi.org/10.1523/JNEUROSCI.1865-13.2014

Jokisch, D., & Jensen, O. (2007). Modulation of Gamma and Alpha Activity during a Working Memory Task Engaging the Dorsal or Ventral Stream. *Journal of Neuroscience*, *27*(12), 3244–3251. https://doi.org/10.1523/JNEUROSCI.5399-06.2007

Kim, S., Kang, J., Choe, S., Jeong, J. W., Kim, H. T., Yun, K., … Lee, S. (2012). Modulation of theta phase synchronization in the human electroencephalogram during a recognition memory task. *Neuroreport*, *23*(11), 637–641. https://doi.org/10.1097/WNR.0b013e328354afed

Koivisto, M., & Silvanto, J. (2012). Visual feature binding: The critical time windows of V1/V2 and parietal activity. *NeuroImage*, *59*(2), 1608–1614. https://doi.org/10.1016/j.neuroimage.2011.08.089

Kopp, F., Schröger, E., & Lipka, S. (2004). Neural networks engaged in short-term memory rehearsal are disrupted by irrelevant speech in human subjects. *Neuroscience Letters*, *354*(1), 42–45. https://doi.org/10.1016/j.neulet.2003.09.065

Kosslyn, S. M., Pascual-Leone, A., Felician, O., Camposano, S., Keenan, J. P., L, W., … Alpert, N. M. (1999). The Role of Area 17 in Visual Imagery: Convergent Evidence from PET and rTMS. *Science*, *284*(5411), 167–170. https://doi.org/10.1126/science.284.5411.167

Kosslyn, Stephen M. (2005). Mental images and the Brain. *Cognitive Neuropsychology*, *22*(3–4), 333–347. https://doi.org/10.1080/02643290442000130

Kosslyn, Stephen M., Thompson, W. L., & Alpert, N. M. (1997). Neural Systems Shared by Visual Imagery and Visual Perception: A Positron Emission Tomography Study. *NeuroImage*, *6*(4), 320–334. https://doi.org/10.1006/nimg.1997.0295

Kottlow, M., Jann, K., Dierks, T., & Koenig, T. (2012). Increased phase synchronization during continuous face integration measured simultaneously with EEG and fMRI. *Clinical Neurophysiology*, *123*(8), 1536–1548. https://doi.org/10.1016/j.clinph.2011.12.019

Lachaux, J.-P., Rodriguez, E., Martinerie, J., & Varela, F. J. (1999). Measuring phase synchrony in brain signals. *Human Brain Mapping*, *8*(4), 194–208. https://doi.org/10.1002/(SICI)1097-0193(1999)8:4<194::AID-HBM4>3.0.CO;2-C

Le Van Quyen, M., Foucher, J., Lachaux, J.-P., Rodriguez, E., Lutz, A., Martinerie, J., & Varela, F. J. (2001). Comparison of Hilbert transform and wavelet methods for the analysis of neuronal synchrony. *Journal of Neuroscience Methods*, *111*(2), 83–98. https://doi.org/10.1016/S0165-0270(01)00372-7

Maris, E., & Oostenveld, R. (2007). Nonparametric statistical testing of EEG- and MEG-data. *Journal of Neuroscience Methods*, *164*(1), 177–190. https://doi.org/10.1016/j.jneumeth.2007.03.024

Mast, F. W., & Kosslyn, S. M. (2002). Eye movements during visual mental imagery. *Trends in Cognitive Sciences*, *6*(7), 271–272. https://doi.org/10.1016/S1364-6613(02)01931-9

Mechelli, A., Price, C. J., Friston, K. J., & Ishai, A. (2004). Where Bottom-up Meets Top-down: Neuronal Interactions during Perception and Imagery. *Cerebral Cortex*, *14*(11), 1256–1265. https://doi.org/10.1093/cercor/bhh087

Melloni, L., Molina, C., Pena, M., Torres, D., Singer, W., & Rodriguez, E. (2007). Synchronization of Neural Activity across Cortical Areas Correlates with Conscious Perception. *Journal of Neuroscience*, *27*(11), 2858–2865. https://doi.org/10.1523/JNEUROSCI.4623-06.2007

Meltzer, J. A., Zaveri, H. P., Goncharova, I. I., Distasio, M. M., Papademetris, X., Spencer, S. S., … Constable, R. T. (2008). Effects of Working Memory Load on Oscillatory Power in Human Intracranial EEG. *Cerebral Cortex*, *18*(8), 1843–1855. https://doi.org/10.1093/cercor/bhm213

Moulton, S. T., & Kosslyn, S. M. (2009). Imagining predictions: mental imagery as mental emulation. *Philosophical Transactions of the Royal Society of London B: Biological Sciences*, *364*(1521), 1273–1280. https://doi.org/10.1098/rstb.2008.0314

Noreika, V., Canales-Johnson, A., Koh, J., Taylor, M., Massey, I., & Bekinschtein, T. A. (2015). Intrusions of a drowsy mind: neural markers of phenomenological unpredictability. *Frontiers in Psychology*, *6*, 202. https://doi.org/10.3389/fpsyg.2015.00202

Nunez, P. L., & Srinivasan, R. (2006). *Electric fields of the brain: the neurophysics of EEG* (2nd ed). Oxford; New York: Oxford University Press.

Nyhus, E., & Curran, T. (2010). Functional role of gamma and theta oscillations in episodic memory. *Neuroscience & Biobehavioral Reviews*, *34*(7), 1023–1035. https://doi.org/10.1016/j.neubiorev.2009.12.014

Oostenveld, R., Fries, P., Maris, E., & Schoffelen, J.-M. (2011). FieldTrip: Open Source Software for Advanced Analysis of MEG, EEG, and Invasive Electrophysiological Data [Research article]. https://doi.org/10.1155/2011/156869

Palva, J. M., Monto, S., Kulashekhar, S., & Palva, S. (2010). Neuronal synchrony reveals working memory networks and predicts individual memory capacity. *Proceedings of the National Academy of Sciences*, *107*(16), 7580–7585. https://doi.org/10.1073/pnas.0913113107

Parkkonen, L., Andersson, J., Hämäläinen, M., & Hari, R. (2008). Early visual brain areas reflect the percept of an ambiguous scene. *Proceedings of the National Academy of Sciences*, *105*(51), 20500–20504. https://doi.org/10.1073/pnas.0810966105

Parra, M. A., Della Sala, S., Logie, R. H., & Morcom, A. M. (2014). Neural correlates of shape–color binding in visual working memory. *Neuropsychologia*, *52*, 27–36. https://doi.org/10.1016/j.neuropsychologia.2013.09.036

Pearson, D. G., Deeprose, C., Wallace-Hadrill, S. M. A., Heyes, S. B., & Holmes, E. A. (2013). Assessing mental imagery in clinical psychology: A review of imagery measures and a guiding framework. *Clinical Psychology Review*, *33*(1), 1–23. https://doi.org/10.1016/j.cpr.2012.09.001

Pearson, J., Naselaris, T., Holmes, E. A., & Kosslyn, S. M. (2015). Mental Imagery: Functional Mechanisms and Clinical Applications. *Trends in Cognitive Sciences*, *19*(10), 590–602. https://doi.org/10.1016/j.tics.2015.08.003

Pollmann, S., Zinke, W., Baumgartner, F., Geringswald, F., & Hanke, M. (2014). The right temporo-parietal junction contributes to visual feature binding. *NeuroImage*, *101*, 289–297. https://doi.org/10.1016/j.neuroimage.2014.07.021

Rodriguez, E., George, N., Lachaux, J.-P., Martinerie, J., Renault, B., & Varela, F. J. (1999). Perception's shadow: long-distance synchronization of human brain activity. *Nature*, *397*(6718), 430–433. https://doi.org/10.1038/17120

Sauseng, P., Griesmayr, B., Freunberger, R., & Klimesch, W. (2010). Control mechanisms in working memory: A possible function of EEG theta oscillations. *Neuroscience & Biobehavioral Reviews*, *34*(7), 1015–1022. https://doi.org/10.1016/j.neubiorev.2009.12.006

Schack, B., Vath, N., Petsche, H., Geissler, H.-G., & Möller, E. (2002). Phase-coupling of theta–gamma EEG rhythms during short-term memory processing. *International Journal of Psychophysiology*, *44*(2), 143–163. https://doi.org/10.1016/S0167-8760(01)00199-4

Shafritz, K. M., Gore, J. C., & Marois, R. (2002). The role of the parietal cortex in visual feature binding. *Proceedings of the National Academy of Sciences*, *99*(16), 10917–10922. https://doi.org/10.1073/pnas.152694799

Stam, C. J., Nolte, G., & Daffertshofer, A. (2007). Phase lag index: Assessment of functional connectivity from multi channel EEG and MEG with diminished bias from common

sources. *Human Brain Mapping*, *28*(11), 1178–1193. https://doi.org/10.1002/hbm.20346

Tallon-Baudry, C., & Bertrand, O. (1999). Oscillatory gamma activity in humans and its role in object representation. *Trends in Cognitive Sciences*, *3*(4), 151–162. https://doi.org/10.1016/S1364-6613(99)01299-1

Tallon-Baudry, C., Bertrand, O., Delpuech, C., & Pernier, J. (1996). Stimulus Specificity of Phase-Locked and Non-Phase-Locked 40 Hz Visual Responses in Human. *Journal of Neuroscience*, *16*(13), 4240–4249. https://doi.org/10.1523/JNEUROSCI.16-13-04240.1996

Vinck, M., Oostenveld, R., van Wingerden, M., Battaglia, F., & Pennartz, C. M. A. (2011). An improved index of phase-synchronization for electrophysiological data in the presence of volume-conduction, noise and sample-size bias. *NeuroImage*, *55*(4), 1548–1565. https://doi.org/10.1016/j.neuroimage.2011.01.055

Yuval-Greenberg, S., Tomer, O., Keren, A. S., Nelken, I., & Deouell, L. Y. (2008). Transient Induced Gamma-Band Response in EEG as a Manifestation of Miniature Saccades. *Neuron*, *58*(3), 429–441. https://doi.org/10.1016/j.neuron.2008.03.027

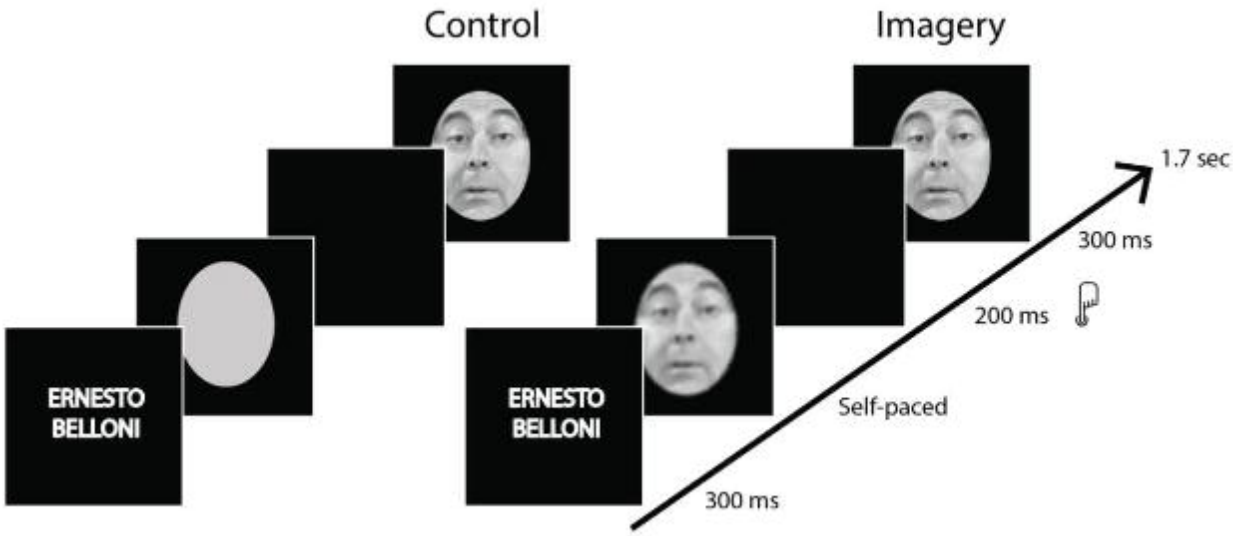
Control
Imagery
ERNESTO
BELLONI
ERNESTO
BELLONI
300 ms
Self-paced
200 ms
300 ms
1.7 sec

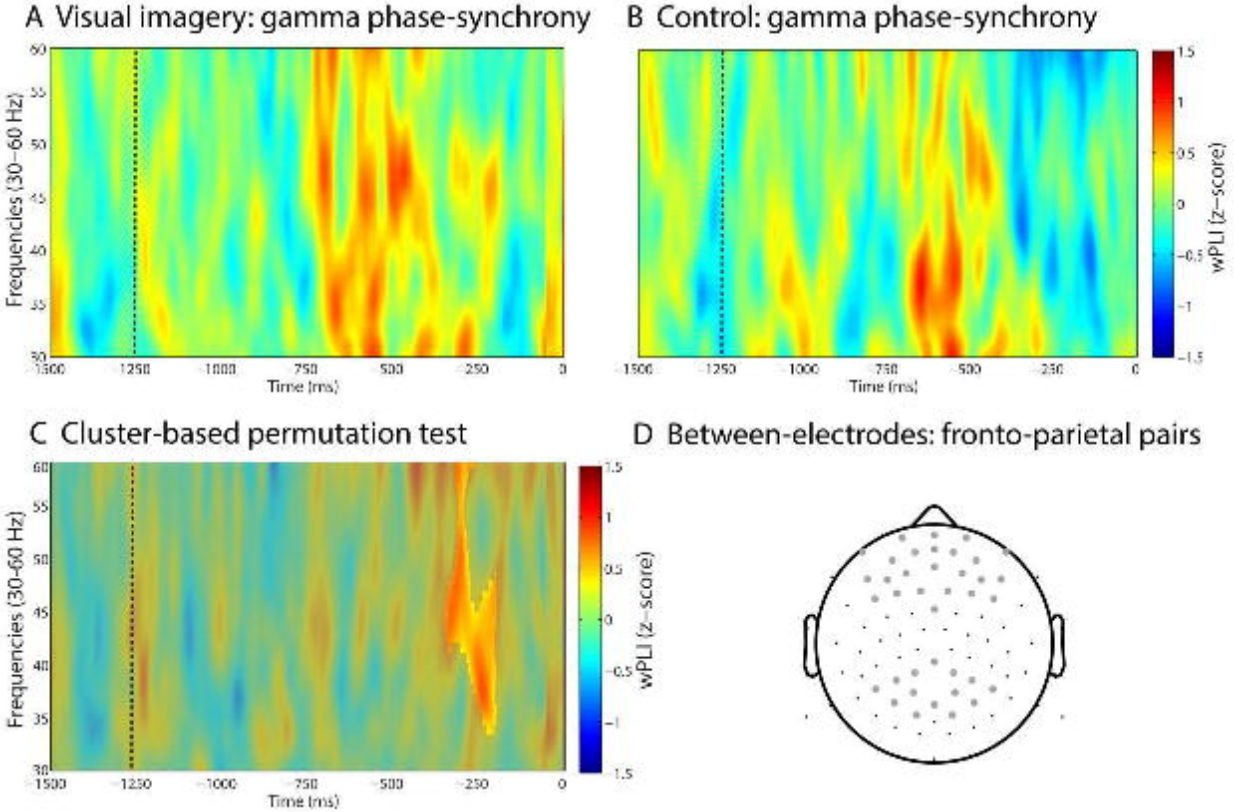
A Visual imagery: gamma phase-synchrony
B Control: gamma phase-synchrony
C Cluster-based permutation test
D Between-electrodes: fronto-parietal pairs
Frequencies (30–60 Hz)
Time (ms)
wPLI (z–score)
-1500
-1250
-1000
-750
-500
-250
0
60
55
50
45
40
35
30
1.5
1
0.5
0
-0.5
-1
-1.5

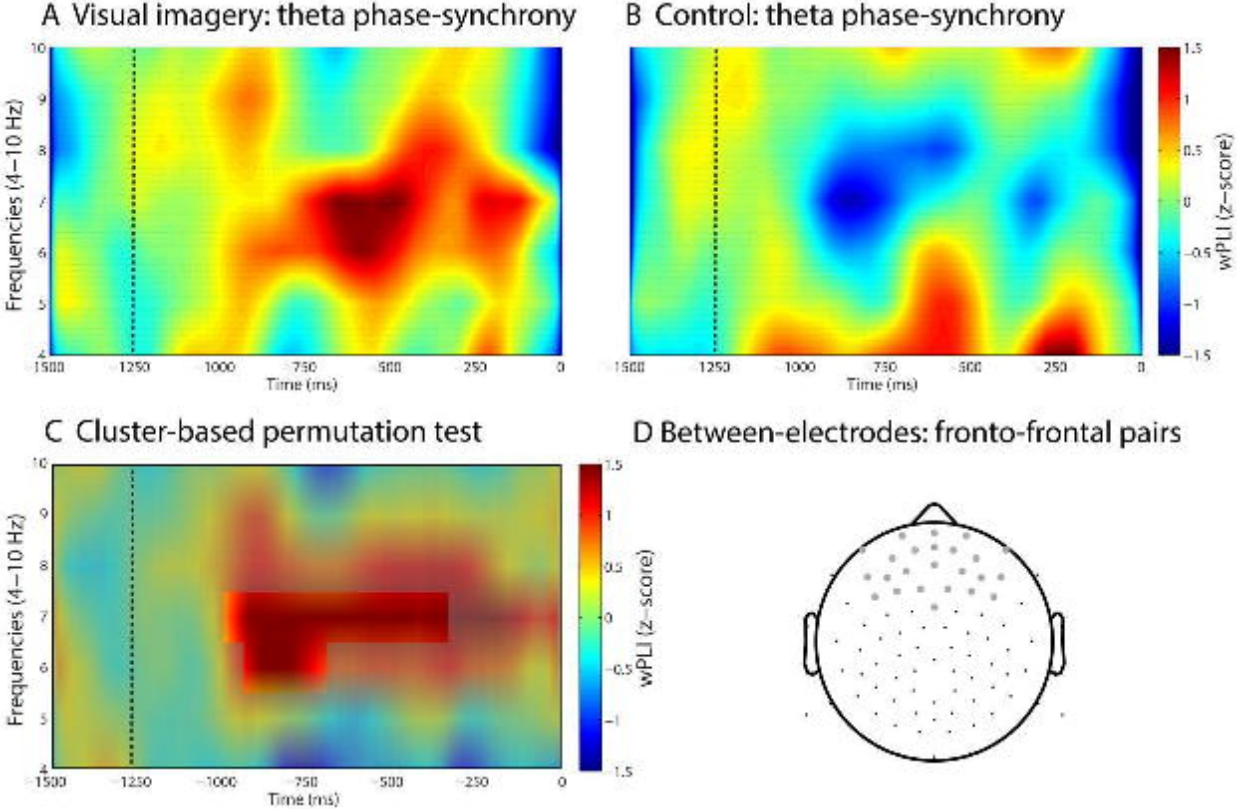
A Visual imagery: theta phase-synchrony
B Control: theta phase-synchrony
C Cluster-based permutation test
D Between-electrodes: fronto-frontal pairs
Frequencies (4–10 Hz)
Time (ms)
wPLI (z-score)
-1500
-1250
-1000
-750
-500
-250
0
10
9
8
7
6
5
4
1.5
1
0.5
0
-0.5
-1
-1.5